Chapter-5

(Auto-combustion processed nano high alumina cements and their implementation as bauxite based low cement castables)

Auto-combustion processed nano high alumina cements and their implementation as bauxite based low cement castables

5.1 Introduction

Iron and steel making industries being the chief consumer of refractories, have made major improvements in the quality and consistency of their products. Demand for structural and clean steel in this century has increased manifold which in turn prompted for better refractories (Rankin and Merwin, 1916; Bray, 1985; Maschio et al., 1988). A significant advancement in refractory technology is hence continually required to meet the service conditions. Evolution of monolithic for a refractory construction in the present day scenario shows a remarkable increase. They offer certain advantages, especially in comparison with shaped articles (Carter, 1961; Skomorovskaya, 1993; Huang et al., 1997). The properties of these castables have been exceedingly better than bricks with comparable chemistries. With the changes in technology, it is now necessary to overcome the limitation of conventional castables (15-20% of calcium aluminate cements) due to its lower high temperature strength, especially when molten slag and metal are present (Bailey and Russel, 1969). The most noticeable improvement in monolithic refractory is low cement/ low moisture castable development (Arlett, 1962). In the new monolithic refractories technology, low and ultra-low cement castables have an ever-decreasing amount of high alumina cement and its corresponding water for placement. Low cement and low water improves high temperature properties. As CaO forms eutectic by slag dissolution, therefore, it became obvious to reduce the CaO content of the castables which meant reducing the cement and water content. To meet the required service condition, the concept of low cement castables was developed (Ownby and Jungquist, 1972). There has been a rapid development in the use of low cement castables in many industries, such as non-ferrous metals, cements, petrochemicals and of course in iron and steel industries (Halloran and Anderson, 1974). These give excellent results in reheating furnaces, ladle linings,

soaking pit bottoms and blast furnace troughs. The superior properties of the low cement castables helped the iron and steel makers to reduce their consumption enormously and hence their operating cost.

Solid state synthesis of calcium aluminates require high temperatures and full conversion is not guaranteed. Moreover, it is difficult to obtain a compositionally homogeneous product with this method. In recent years, combustion synthesis has attracted a great deal of attention to produce superfine, un-agglomerated, multicomponent crystalline ceramic without intermediate decomposition or calcination (Fumo et al., 1996). This method exploits an exothermic, rapid and self-sustaining chemical reaction. Its key feature is that the reaction itself provides the heat required to drive the chemical reaction without any external source (MacZura et al., 1985, Gulgun et al., 1994; Hall et al., 2004).

Commercial high alumina cements are known to contain various phase viz., CA, CA_2, $C_{12}A_7$ and α-alumina whose hydration behavior is interdependent and not yet fully understood (Singh and Ali, 1980; Singh and Mandal, 1982; Mukhopadhyaya and Das Poddar, 2004). The mono calcium aluminate (CA) imparts high mechanical strength and refractoriness to the cement, where rapid setting is mostly associated with $C_{12}A_7$ which dissolves rapidly (Perez et al., 1983; Scrivener and Capmas, 2004; Klaus et al., 2013). Cement with high amount of CaO has many drawbacks when used as hydraulic binders in refractory castables due to their excess water demand during casting process, porosity due to drying as well as their low refractoriness when it comes in contact with SiO_2.

There has been enormous amount of work in the field of solution derived combustion of calcium aluminates, however there is lack of studies which focus on their utilization as castables. The work presented in this chapter opens new doors by implementation of prepared cement as monoliths and to optimize their hot properties. The first part of the work describes the synthesis of high alumina cements (CA, CA_2 and $C_{12}A_7$) by the auto combustion reaction of redox mixtures of the corresponding water-soluble nitrate salts with urea. For reference study, a

comparison with commercial high alumina cement is reported herein. In the second stage of work, formulation as well as characterization of bauxite castables and prepared cement as the binder is discussed to assess and achieve a good quality of low cement castable. Together, the aluminates and the micro fillers are responsible for the hydraulic setting of the castable. With packing density maximized, the low cement castables are characterized by their low porosity, high density and exceptional hot strength; with enhanced erosion, corrosion, and spalling resistance (Wrust and Nelson, 1972; Singh et al., 1990; Masaryk et al., 1993).

5.2 Experimental procedure

5.2.1 Material characterization

The starting raw materials of A.R. grade such as aluminum nitrate $Al(NO_3)_3.9H_2O$, calcium nitrate $Ca(NO_3)_2.4H_2O$, urea $(NH_2)_2CO$, chromium oxide (Cr_2O_3) and magnesium oxide (MgO) powder were supplied by Loba Chemie Pvt. Ltd., Mumbai, India. The calcined Chinese bauxite that was used in castable formulation in the present study, contained approximately 88.60%, 4.78%, 1.58%, 4.0%, 0.26%, 0.08% and 0.70% by weight Al_2O_3, SiO_2, Fe_2O_3, TiO_2, CaO, Na_2O and others respectively, as specified by the supplier (Shiva Minerals, Rourkela, India).
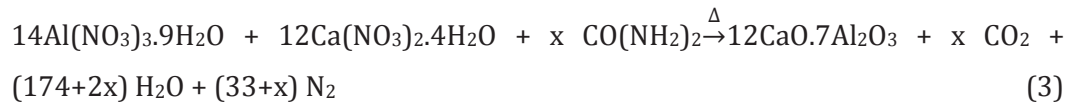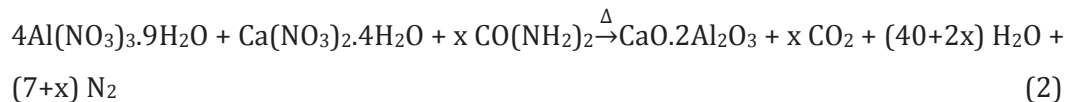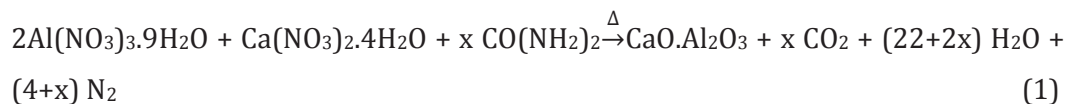
5.2.2 HAC powder preparation

Combustion synthesis or self-propagating high temperature synthesis is a versatile method, used for the synthesis of a variety of solids. The method makes use of a highly exothermic reaction between the reactants to produce a flame due to spontaneous combustion which then yields the desired product or its precursor in finely divided form. In order for combustion to occur, initial mixture of reactants should be highly dispersed and must have high chemical energy. Even if the desired product is not formed immediately after combustion, the fine particulate nature of the product facilitates its formation by further heating. Reaction times are very short since the desired product results soon after the combustion.
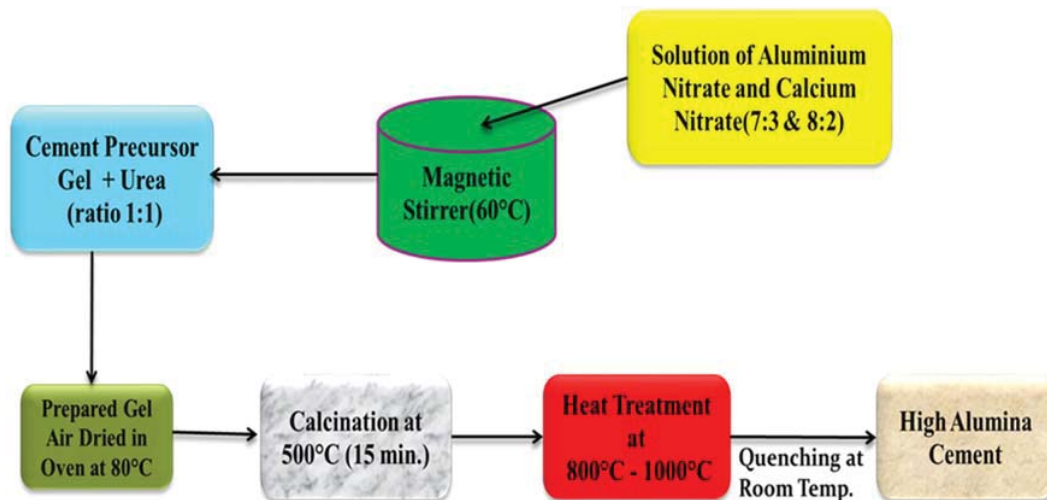
The auto-combustion synthesis technique consists of bringing a saturated aqueous solution of the desired metal salts and a suitable organic fuel to boil, until the mixture ignites and a self-sustaining and rather fast combustion reaction takes off, resulting in a dry, usually crystalline oxide powder. While redox reactions such as this are exothermic and often lead to explosion if not controlled, the combustion of metal nitrates and urea mixtures usually occurs as a self-propagating and non-explosive exothermic reaction. The large amounts of gases formed can result in visible flame, which can reach temperatures above 1000℃.

Aluminum nitrate $Al(NO_3)_3.9H_2O$ and calcium nitrate $Ca(NO_3)_2.4H_2O$ were weighed and mixed on a laboratory scale in a weight ratio of 7:3 and 8:2 of Al_2O_3/CaO, which were denoted as HAC70 and HAC80 respectively. For complete dissolution of the salts, the solution was kept on a hot plate at around 60°C with simultaneous stirring until a clear transparent solution was obtained. To this precursor solution, urea was poured keeping a cement precursor/fuel ratio of 1:1. The prepared gel was air-dried in an oven at 80°C to complete dryness. Finally, after the solution was converted to a dried gel powder, it was calcined for 15 minutes in air at 500°C with subsequent quenching to room temperature. During the first few minutes of the calcinations process, ignition took place with a rapid evolution of large amounts of gases. Therefore, only small portions of the gels were calcined. The synthesis technique use the heat energy released by the redox exothermic reaction at a relatively low ignition temperature between metal nitrates and urea. The process lasted for a relatively short time, so that the particles could be maintained to the nanometer scale. Further high alumina cements nano composite powders were heated at 800 and 1000°C in a platinum dish using a SiC muffle furnace for a soaking period of 2h. After complete heating processes, the HAC powders were stored in air sealed desiccator.

The probable chemical reactions are given below:

$$2Al(NO_3)_3.9H_2O + Ca(NO_3)_2.4H_2O + x\ CO(NH_2)_2 \xrightarrow{\Delta} CaO.Al_2O_3 + x\ CO_2 + (22+2x)\ H_2O + (4+x)\ N_2 \tag{1}$$

$$4Al(NO_3)_3.9H_2O + Ca(NO_3)_2.4H_2O + x\ CO(NH_2)_2 \xrightarrow{\Delta} CaO.2Al_2O_3 + x\ CO_2 + (40+2x)\ H_2O + (7+x)\ N_2 \tag{2}$$

$$14Al(NO_3)_3.9H_2O + 12Ca(NO_3)_2.4H_2O + x\ CO(NH_2)_2 \xrightarrow{\Delta} 12CaO.7Al_2O_3 + x\ CO_2 + (174+2x)\ H_2O + (33+x)\ N_2 \tag{3}$$

Figure 5.1: Flow chart of HAC powder preparation.

5.2.3 Castable formulation

Low cement refractory castables were prepared using approximately 5 wt. % HAC and rest contents were refractory grade bauxite and certain additives. In the first step for cement castable formulation, calcined bauxite was oven dried, crushed and ground for grading into different sizes in a planetary ball mill. The jar and grinding media were of titanium-coated stainless steel material. At one time 300 gm of calcined bauxite material was taken in a jar and grounded in a high energy planetary ball mill for 15 min at 600 rpm. Similarly, it was processed to complete the grinding of complete material. The ground material was then kept in various selected sieves and set up on the motorized vibro-sieving equipment for grading. After separation of different graded bauxite, experiments were performed further to study the nature of ultra-fine particles on high temperature properties like creep behavior, corrosion resistance and hot strength. The trials of aggregate proportions were taken in a 1000 cm^3 flask filled up to 250 cm^3 and vibrated for 30 sec and the packing density calculations were carried out for each trial. Aggregates having higher packing densities were chosen for further analysis. In the next step, batches were prepared

by taking different grades of materials and additives in the proper proportion and are summarized in Tables 5.1 and 5.2. The materials were dry mixed in a plastic container for 10 min with a spatula and then were taken for sample preparation. Generally, ultra and LCCs require less than 5 wt. % of water to achieve the desired rheology; therefore, water was added in two steps. The casting was done by adding the first two-thirds proportion of water at a time. Then, one-third of water was added slowly to get a homogeneous mixing. The wet mixing was performed for up to 5-6 min to achieve proper flow. Immediately after wet mixing, the castable mix was filled into a rectangular bar shape mould (152 mm × 25 mm × 25 mm) made of hard steel. The mould was placed on the vibrating table filled with the wet mixed castable and the mixes were vibrated for 10 min, resulting in better compactness. For each composition, several samples were prepared for laboratory test. The samples were cured in a moisture-saturated environment (95% RH) in a humidity chamber at room temperature for different time periods. For firing the samples, they were first oven dried at 110 °C for 24 h. The test samples were fired at 1300-1550 ±5 °C in an electric furnace, with SiC heating element and a soaking time of 3h. The cured samples as well as the fired samples were tested for their bulk density, apparent porosity (ASTM C20-00), HMOR (ASTM C583-10), CMOR (ASTM C133-97) and cold crushing strength (ASTM C1194-03). These samples were also analyzed by XRD for phases present and by SEM for their morphological behavior.
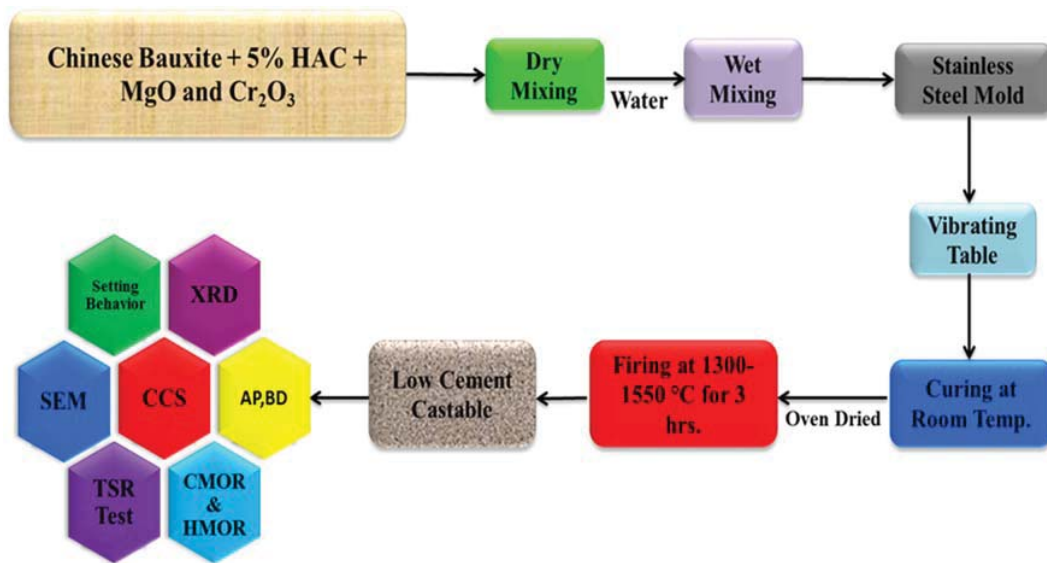
Figure 5.2: Low cement castable preparation.

Table 5.1: Batch composition with HAC70.

Sample	HAC70 (Wt %)	Chinese Bauxite (Wt %)	Microfine MgO (Wt %)	Microfine Cr_2O_3 (Wt %)
P1	5	85	9	1
P2	5	85	8	2
P3	5	85	7	3
P4	5	85	6	4
P5	5	85	5	5
P6	5	85	4	6
P7	5	85	3	7
P8	5	85	2	8

Table5.2: Batch composition with HAC80.

Sample	HAC80 (Wt %)	Chinese Bauxite (Wt %)	Microfine MgO (Wt %)	MicrofineCr$_2$O$_3$ (Wt %)
Q1	5	85	9	1
Q2	5	85	8	2
Q3	5	85	7	3
Q4	5	85	6	4
Q5	5	85	5	5
Q6	5	85	4	6
Q7	5	85	3	7
Q8	5	85	2	8

5.2.4 Cold crushing strength of HAC and LCC formulated

The CCS is the capacity of a material to withstand axially directed pushing forces. By definition, the compressive strength of a material is that value of uniaxial compressive strength reached when the material fails completely. CCS of cement was measured as the compressive strength of a 50 mm cement cube made of pure HAC (without any aggregates).These samples were tested for compressive strength after 6 h, 24 h and 48 h, respectively according to (ASTM C1194-03).

5.2.5 Cold and hot modulus of rupture (CMOR and HMOR) of LCC formulated

Cold and hot modulus of rupture (CMOR and HMOR) measurements were carried out under three-point bending tests (ASTM C133-97 for CMOR and ASTM C583-10 for HMOR) using 152mm × 25mm × 25mm samples. CMOR and HMOR were calculated using the following formula:

$$MOR = \frac{3PL}{2db^2}$$

where,

MOR = modulus of rupture (MPa),

P = maximum applied at rupture (N),

L = span between supports (mm),

b = breadth or width of specimen (mm), and

d = depth of specimen (mm).

CMOR tests were conducted at room temperature using Universal Materials Test Equipment (Model 810, MTS System, Eden Prairie, MN, USA) for samples pre-fired at 1300°C, 1350°C, 1400°C, 1450°C, 1500°C and 1550°C for 3h. HMOR measurements were made at 1400°C, 1500°C and 1600°C using Netzsch 414/3 HMOR Equipment (Netzsch, Selb, Germany) for samples pre-fired at 1550 °C for 3 h, cooled at room temperature and then reheated for testing.

5.3 Results and discussion

5.3.1. Evolution of phases by X-Ray diffraction

Figures 5.3 and 5.4 are the XRD patterns of samples having 70% and 80% alumina termed as HAC70 and HAC80, respectively, calcined at 800°C and 1000°C. The effect of calcination for a period of 2h at 800°C and 1000°C were investigated. For all the aluminates, calcining steps at high temperatures only promote the degree of crystallinity and grain growth. The mixtures were ignited as soon as they were placed inside the pre-heated furnace at 500°C. The reactions were rapid and produced greyish white and lacy dry foams, accompanied by a great volume increase. But the temperature was not enough to promote the crystallization of the desired phases. When calcined below 800°C, these powders proved to have an X-ray pseudo-amorphous pattern, where the initial formation of calcium-aluminate phases may be envisaged. When calcination temperature was brought up to 1000°C, sign of the crystalline aluminate was detected in the X-ray diffraction pattern. In spite of the short reaction time, X-ray diffraction of the prepared powders portrayed well crystallized CA, CA_2, and $C_{12}A_7$ (full conversion), as these were only phases present at 1000°C. Prime phases investigated in both cases are readily formed and thermodynamically most stable compounds in the CaO-Al_2O_3 binary system. These peaks were identified by standard JCPDS cards numbered 41-0359, 34-0442 and 09-0412 for their corresponding peaks of hexagonal CA, monoclinic CA_2 and cubic $C_{12}A_7$, respectively. In the conventional preparation route by high-temperature solid-state synthesis, the batch usually has CaO-rich phases and un-reacted Al_2O_3 before the desired product phase appears. The formation sequence of phases in these mixtures is always from calcia-rich phase to the alumina rich phase, which could be accounted for $C_{12}A_7$ formation, as soaking period was very low. Presence of broad peaks in XRD patterns of calcined cement powders shows that particle size is small. Crystallite size, d of calcined powder was calculated from X-ray line broadening analysis using Scherer's formula:

$$d = \frac{0.9\lambda}{\beta \cos\theta}$$

where, β is the full width at half maximum (FWHM) intensity of a Bragg reflection excluding instrumental broadening, λ is the wavelength of the X-ray radiation and θ is the Bragg angle. β is taken for the strongest Bragg's peak corresponding to 2θ. Both samples have crystallite size in the range of 18-38 nm.

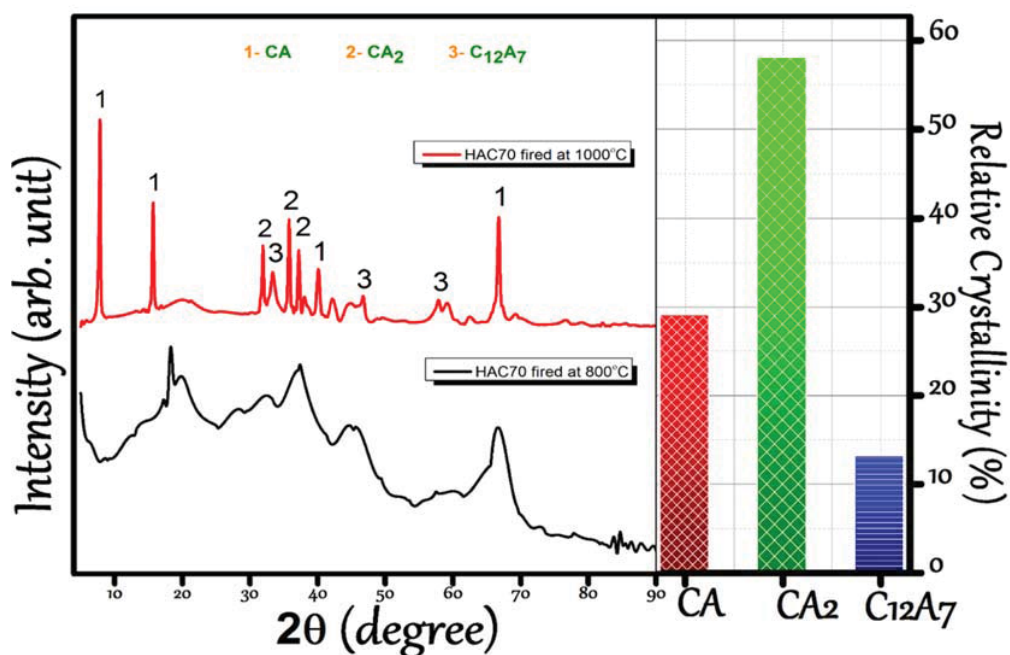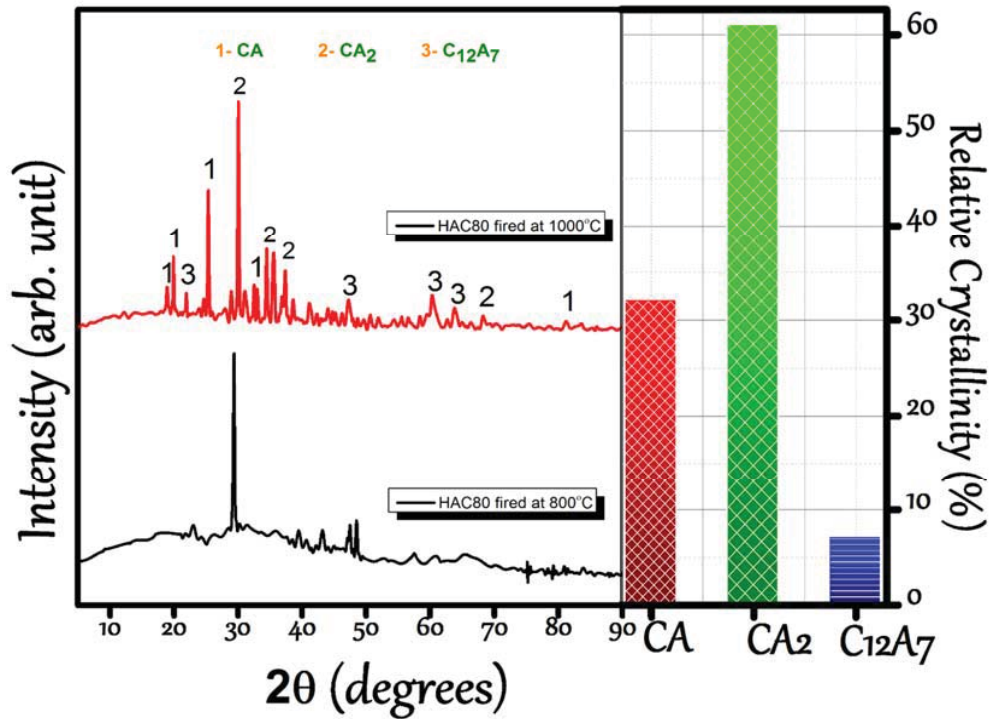**Figure 5.3: XRD plot of HAC70.**

Figure 5.4: XRD plot of HAC80.

5.3.2 Setting behavior of HAC

Figure 5.5 shows the setting behavior of HACs. The prepared and finely ground HAC powders were mixed with water (0.85 P). The initial possible hydration products of calcium aluminate cement are CAH_{10} and C_2AH_8. With the passage of time these products are replaced by C_3AH_6 and AH_3 at rates that depend on the temperature and other factors; this process is called conversion. Generally an amorphous or gel phase containing Ca^{2+} forms simultaneously with the crystalline products. In the subsequent course of the reaction, an induction period occurs during which the concentrations remain near their maximum values. The rates of dissolution and precipitation thus being approximately equal. The precipitation products nucleate and grow; these processes begin slowly, but accelerate with time. Ultimately, precipitation is massive with the concentrations drop and in a paste, setting occurs. In the conversion reaction, CAH_{10} and C_2AH_8 re-dissolve and C_3AH_6 is formed,

together with additional AH_3. The structure of which then approximately equivalent to that of gibbsite. At room temperature, 70% alumina containing cements gave an initial setting time of 22 min and final setting occurred in 52 min. Another composition of HAC, having 80% alumina, had an initial setting time of 24 min with a final setting time of 67 min. With increasing alumina content in HAC, the setting time showed an increasing trend.
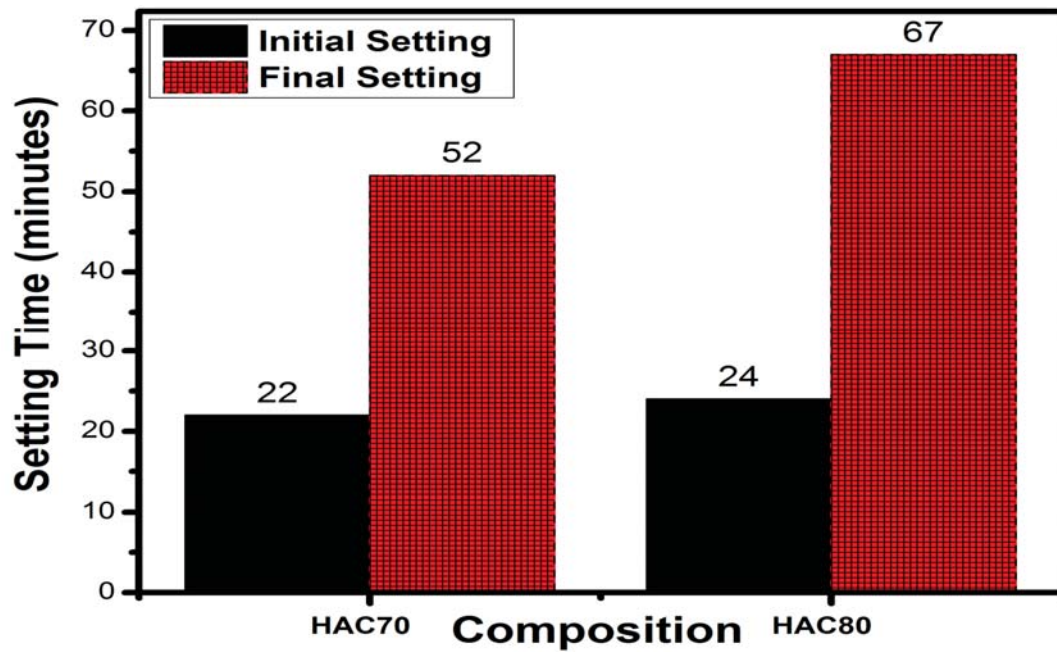

Figure 5.5: Setting time behavior of HAC70 and HAC80.

5.3.3 CCS of HAC fired at 1000°C

The pure (without any aggregates) HAC samples attained good structural strength in the present experimental work and are shown in figure 5.6. Samples were tested after curing for 6h, 24h and 48h. Sample blocks with the inclusion of two commercialized cements of similar compositions were prepared to have a comparative study. The strength increased rapidly with curing time in all the compositions. In high alumina containing cement system, saturation of $Al(OH)_4^-$ ions lead to an increase of the pH and the ionic strength of the aqueous medium. This reduces the hydration rate at early ages and high early strength is not achieved until nuclei of calcium aluminate hydrates are formed. Eventually the formation of denser stable hydrates (C_3AH_6 and AH_3) occurs. So, initially, in 6 h, the CCS value obtained for HAC70 is 10 MPa and for HAC80 is 12 MPa. After 48 h it reached up to 65 and 72MPa for HAC70 and HAC80, respectively. These values were better than the commercially available CA-14M (55MPa) and CA-25C (50 MPa). It gets the maximum strength at around 48h and after this period there is a very slight variation. It can be seen that HAC80 samples have more compressive strength than the HAC70 sample. The higher strength of HAC80 is ascribed to the presence of larger amounts of CA and CA_2. It is well-known that CA and $C_{12}A_7$ react significantly in the early ages of hydration with remarkable exothermic hydration of $C_{12}A_7$. Therefore, the formation of stable hydrates generally occurs sooner. Although CA_2 is known to react slowly with water in the early stages of hydration, its presence along with other phases results in an overall faster hydration rate as the heat of hydration resulting from the hydration of CA activates CA_2 and makes it react relatively faster with water than it would do alone. CCS data of the sintered ceramic bodies exhibit high strength of both samples. This is due to the formation of the ceramic bond and the absence of any impure phase.
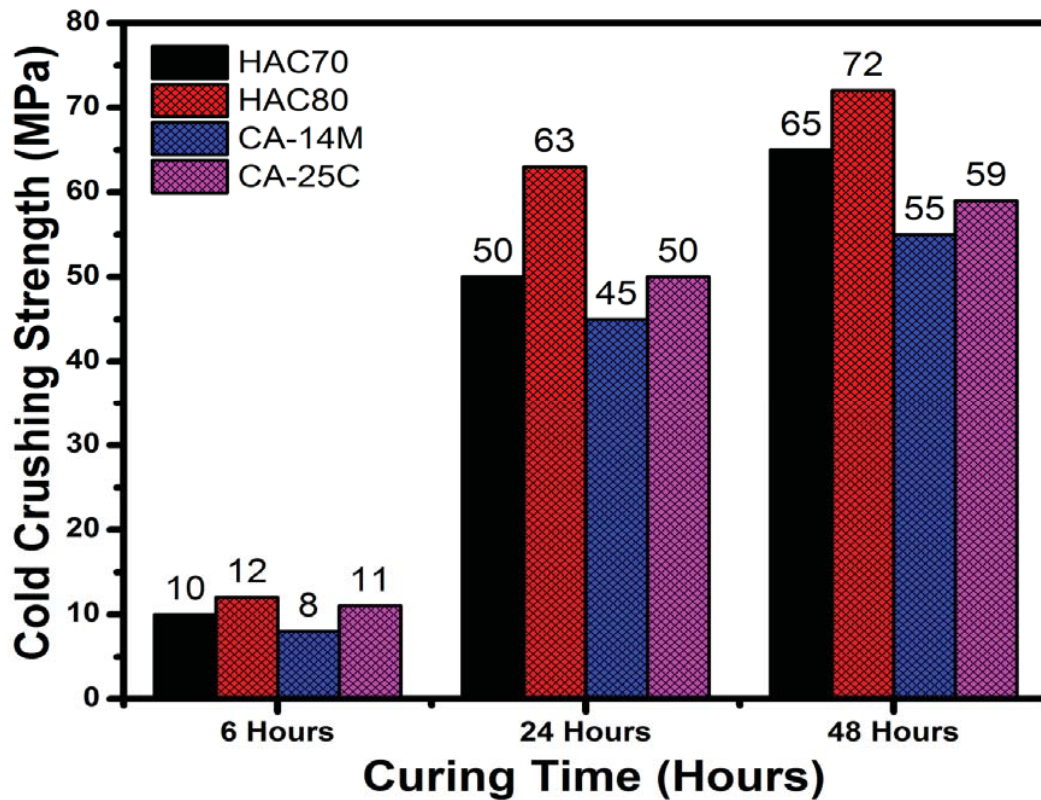
Figure 5.6: Cold crushing strength of HAC70 and HAC80.

5.3.4 SEM of high alumina cement

Figures 5.7 and 5.8 represent the SEM of HAC70 and HAC80 samples, respectively, fired at 1000°C. Networks of well-crystallized interlocking hexagonal plates of CA matrix in both figures can be seen, where a, b, c and d represent micrographs at different magnifications of same sample. The monoclinic phases of CA_2 and cubic $C_{12}A_7$ can be observed in both figures. CA produced here has the finest particles with euhedral crystals loosely agglomerated. CA_2 crystals are similar in shape but larger and the agglomerates show signs of incipient sintering. $C_{12}A_7$ crystals, on the contrary, in spite of crystallizing in the cubic system, are of needle like shape and enveloped by a transparent sheath, suggesting that nuclei grow from a glassy

material. The higher amount of CA and CA_2 is proposed to enhance the refractory properties. $C_{12}A_7$ phase is responsible for high bonding and quick hydration and small cubic crystals of this phase are evident in the most homogeneous distribution of the CA phase matrix.
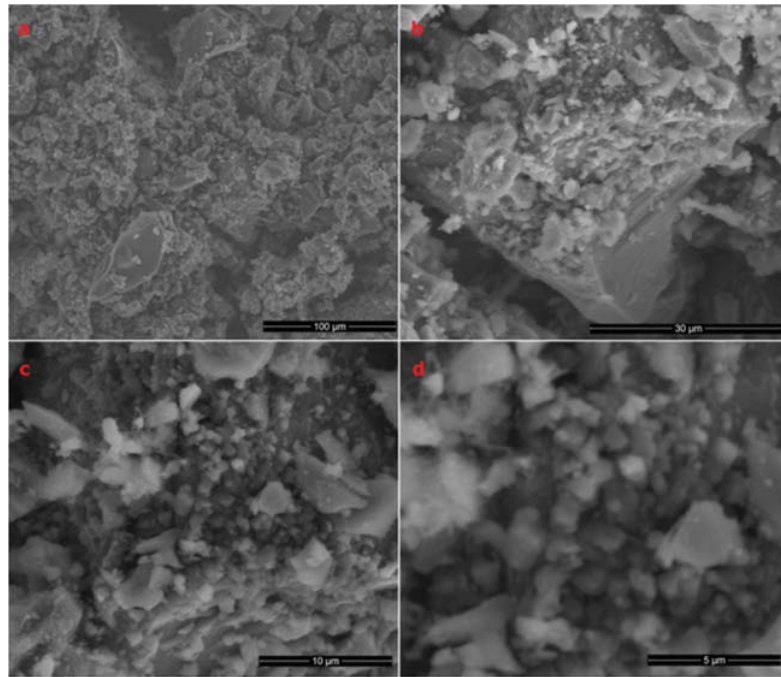
Figure5.7: SEM of HAC70.
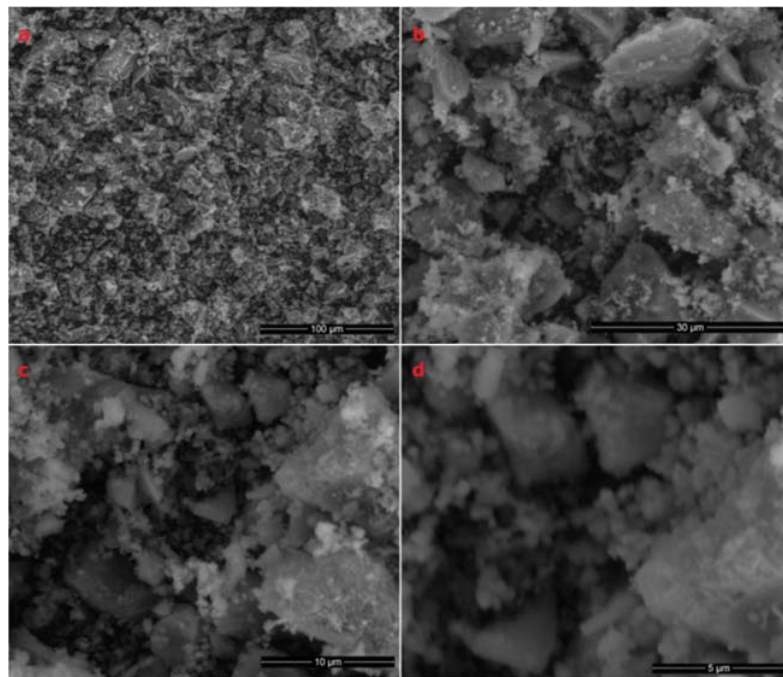
Figure 5.8: SEM of HAC80.

5.3.5 XRD patterns of castables fired at 1550°C for 3 h

Figures 5.9 and 5.10 portray XRD patterns of castables fired at 1550°C for 3h. Here P1 to P8 and Q1 to Q8 indicate castables formulated with HAC70 and HAC80, respectively. The corundum phase appeared as a major component due to the transformation of bauxite minerals to corundum. The second major phase was detected as spinel ($MgAl_2O_4$). Appearance of $MgCr_2O_4$ spinel also occurred as a minor peak which resulted due to the interaction of MgO and Cr_2O_3 in all the castable samples. In both castable series P and Q, as we proceed from high to low batch number, the peak intensities of spinel increase which is accounted for increased micro fine MgO and Cr_2O_3 content. These peaks were identified by standard JCPDS cards numbered 81-2267, 82-1529, 77-438 and 89-4203 for figure 5.9 and 89-7716, 82-1529, 86-0095, 89-4921 for figure 5.10.
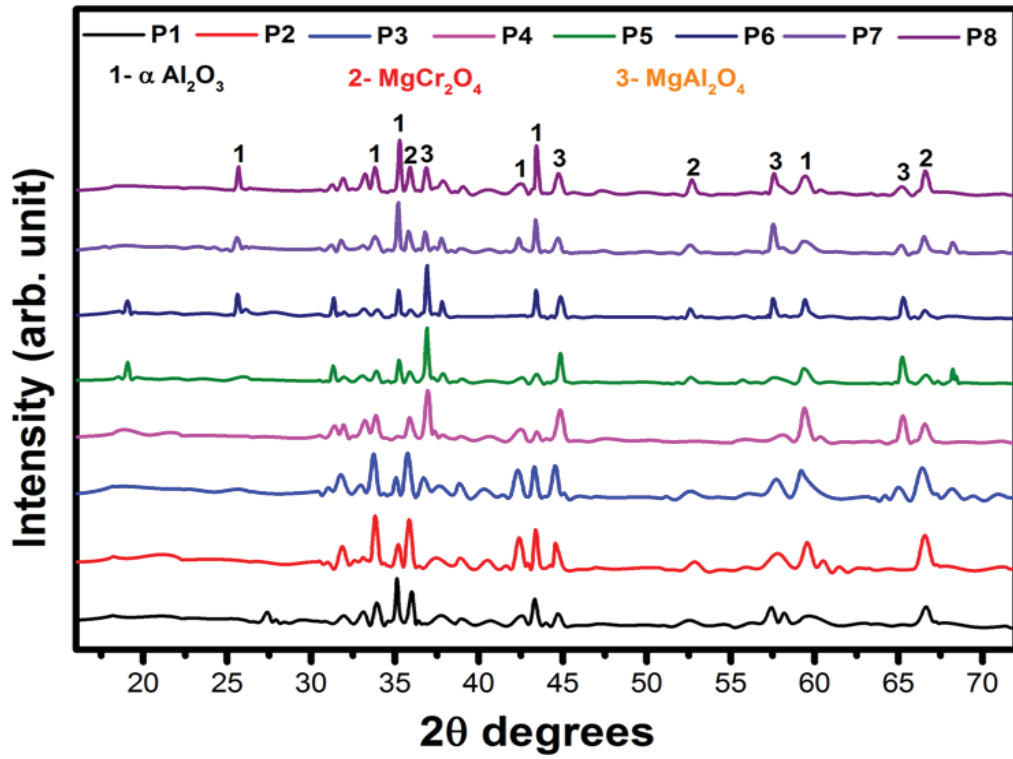
Figure 5.9: XRD plot of P series castables prepared with HAC70.
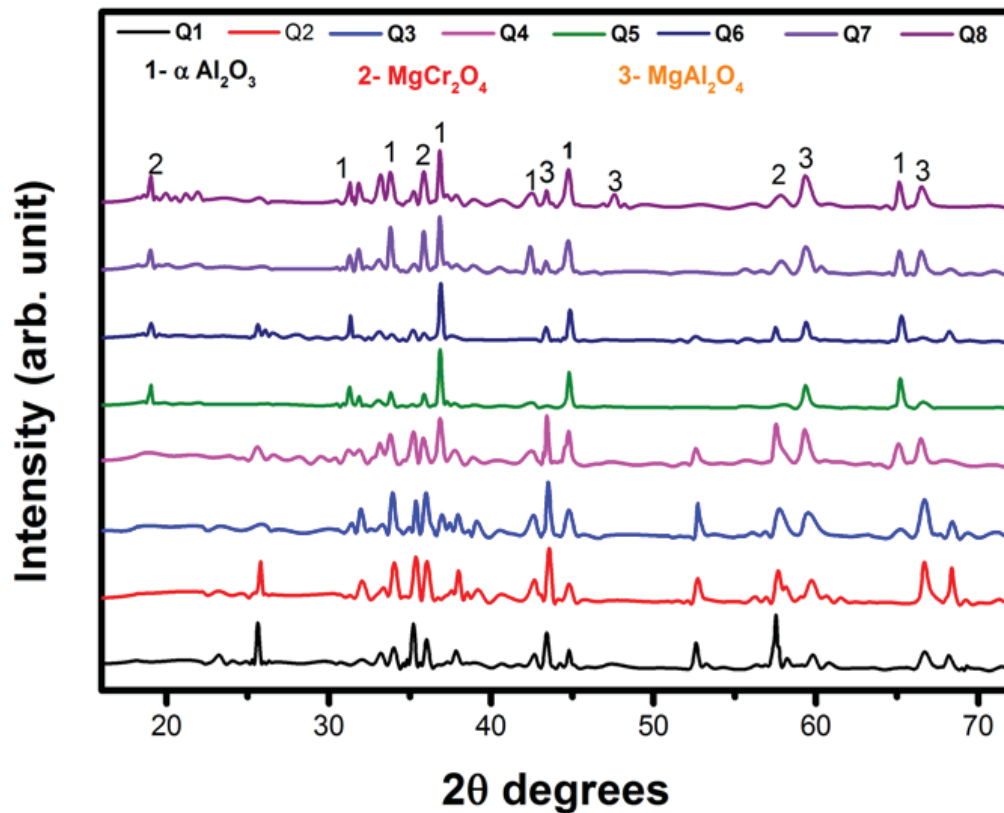
Figure 5.10: XRD plot of Q series castables prepared with HAC80.

5.3.6 Bulk density, apparent porosity and thermal shock cycles of prepared castables

Table 5.3 shows the values corresponding to bulk density, apparent porosity and thermal shock of P2 and Q2 series castables, sintered at various temperatures. Only these series were selected due to their thermo-mechanical superiority. In the prepared castables, highest bulk densities achieved were 3.21g/cm^3 and 3.32 g/cm^3 for the compositions P2 and Q2, respectively. This can be attributed to the use of higher percentages of alumina and micro-fine MgO, which lead to in-situ spinel formation. The densification can also be attributed to Al_2O_3-Cr_2O_3 system which forms substituted solid solution $(Al_{2-x}Cr_x)_2O_3$ $(0 \leq x \leq 2)$ over an entire range of composition at high temperatures without formation of any eutectic. They have the corundum crystal structure, consisting of a hexagonal close packed array of oxygen

anions with two-third of the octahedral interstitials occupied by the cations (Nath et al., 2013). Apparent porosity was measured to be in the range of 8%-10.69% in all the castables prepared. Table 5.3 displays the thermal shock cycle values evaluated for Q2 and P2 series castables. This series was chosen in accordance with their superior thermo-mechanical properties.

Thermal-shock resistance tests were run to analyze the influence of the corundum and spinel content and the characteristics on the thermal-mechanical properties of castables. The tests consisted of 10 heating/cooling cycles (DT = 1200 °C). The thermal shock is the generation of thermo-mechanical stresses in the material due to the sudden change in temperature. When the tensions generated are greater than the breakdown strain of the material, nucleation and crack propagation occurs, damaging the structure of the material. Samples completed one thermal cycle after a holding time of 20 min inside the furnace at predetermined, followed by another 20 min of cooling in air at room temperature. All the Q and P series samples exhibited high thermal shock and spalling resistance on completing 12 cycles; while Q2 and P2 attained 18 and 16 cycles, respectively. Such high spalling resistance is attributed to irregular in-situ spinelization, which inhibits the crack development and growth due to abrupt temperature changes.

Table 5.3: Bulk density, apparent porosity and thermal shock cycles of prepared castables.

Test Method	Temperature (°C)						
	Sample Name	1300	1350	1400	1450	1500	1550
Bulk Density (gm/cc)	P2	2.75	2.90	3.00	3.05	3.20	3.21
	Q2	2.80	2.95	3.10	3.15	3.29	3.32
Apparent Porosity (%)	P2	10.69	10.61	9.91	9.80	9.20	9.00
	Q2	8.90	8.80	8.60	8.50	8.15	8.00
Thermal Shock Cycle	P2	15	14	14	15	15	16
	Q2	14	16	14	15	16	18

5.3.7 CCS of different castable compositions sintered at 1300°C-1550°C for 3 h

Prepared HAC powders were used for formulating LCC according to the Tables 5.1 and 5.2. Micro fine MgO and Cr_2O_3 content have been varied, which resulted in varying amount of corundum and spinel phase formation. These reactions also have a varying effect in the CCS values of the castables formulated in above mentioned manner. Figure 5.11 depicts the CCS of castables series Q and P. High values of CCS up to 151-285 MPa was achieved at the maximum sintering temperature of 1550°C for Q series castables. Similarly, CCS value in the range of 145-279 MPa was achieved for P series castables. It may be predicted that the rise in sintering temperature gives interlocking types of grains, thus reducing inter-granular porosity. This has a positive effect on the mechanical properties of both series of castables. Formation of spinel strengthens the structure at high temperature and mullite solid solution helps in increasing densification. The CCS of the castables prepared with HAC70 and HAC80 were higher in comparison with the CCS of

conventional bauxite containing LCC containing Secar-71(140 MPa) and Secar80 (200 MPa).
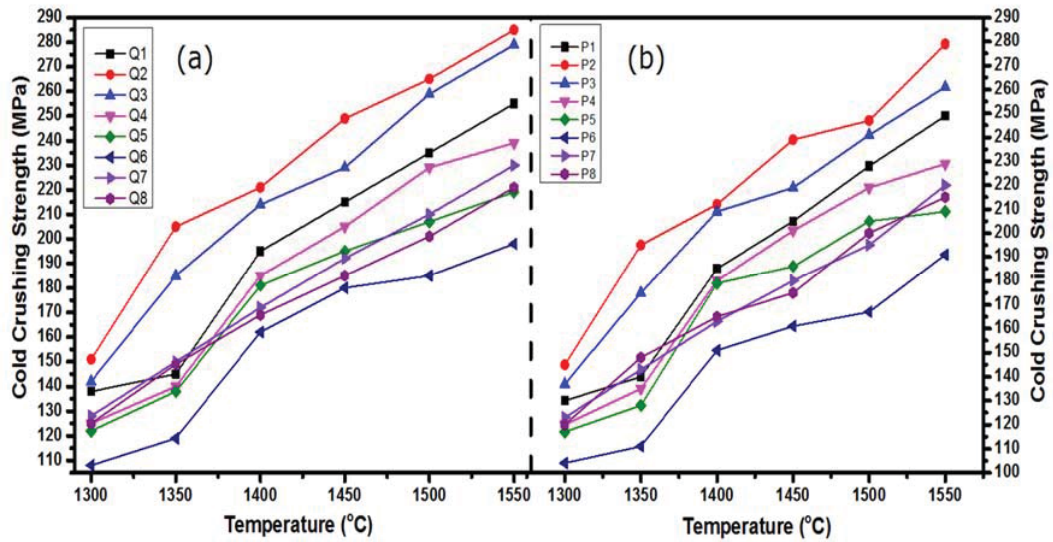

Figure 5.11: (a) Cold crushing strength of Q series of castables; (b) Cold crushing strength of P series of castables.

5.3.8 CMOR and HMOR of different castables

Cold modulus of rupture strength (CMOR) of castables Q and P series is shown in figure 5.12. It can be seen that CMOR of both series castables has increased with the increasing sintering temperature and was maximum for Q2 in which maximum amount of corundum and spinel grains was formed. $MgO\text{-}Cr_2O_3$ spinelisation could also be accounted for higher mechanical properties as this reaction has an expansive nature, hence the micro-cracks generation plays a positive role in strength development. This was reflected in the strength of the whole castable samples. Hot modulus of rupture (HMOR) of castables Q and P series is shown in figures 5.13 and 5.14, respectively. Here, again Q2 achieved the maximum strength at high temperature/load. The increase in HMOR values of some samples in temperature range of 1400 to 1600°C is due to the formed magnesium aluminate spinel and alumina-chrome solid solutions. CaO in the cement is favorable for the presence of a liquid phase at high temperatures, which helps to accommodate thermo-mechanical stresses generated and thereby, improving hot properties. High-temperature tensile ductility in fine-grained Al_2O_3 is an extensively researched phenomena which is enriched by small amounts of secondary phases. For enhancement of this phenomenon, suppression of alumina grain growth and co-dispersion of spinel, magnesia or zirconia particle is required. The reaction derived in-situ spinel, as observed through XRD patterns, here acts as dispersive agent in corundum. Due to this superplastic behavior, rise in the high temperature bending strengths is observed when magnesia is added incrementally. Abnormal grain growth of bauxite is suppressed as is seen by microstructural plots, even though densification is not hampered. To conclude from this result, we may say that the safe range for these types of castables at higher loads is lower than 1600°C. The impurities in the bauxite aggregate also increase the liquid phase at sintering temperature and decrease the porosity which consequently increases the mechanical properties.
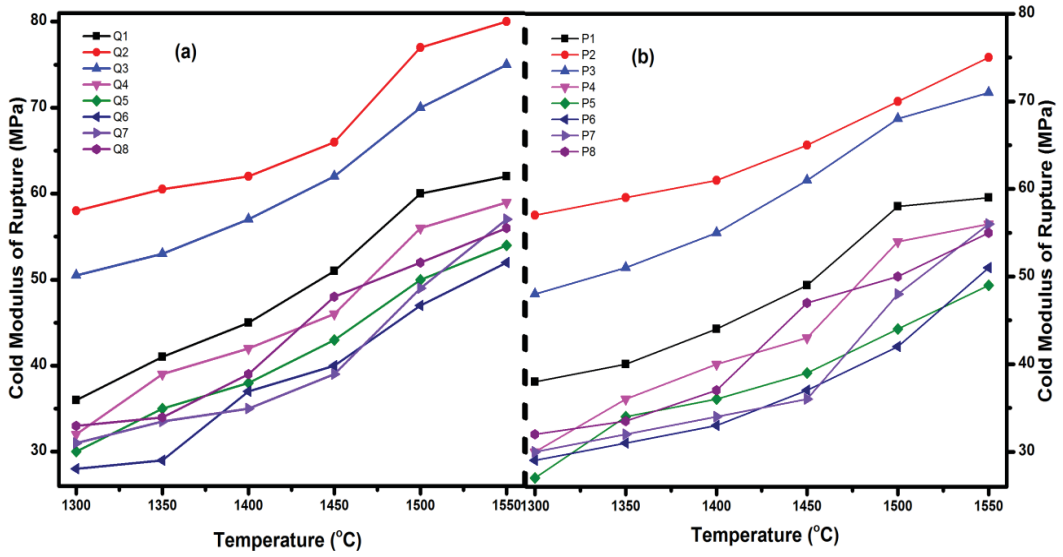
Figure 5.12: (a) Cold modulus of rupture of Q series of castables; (b) Cold modulus of rupture of P series of castables.
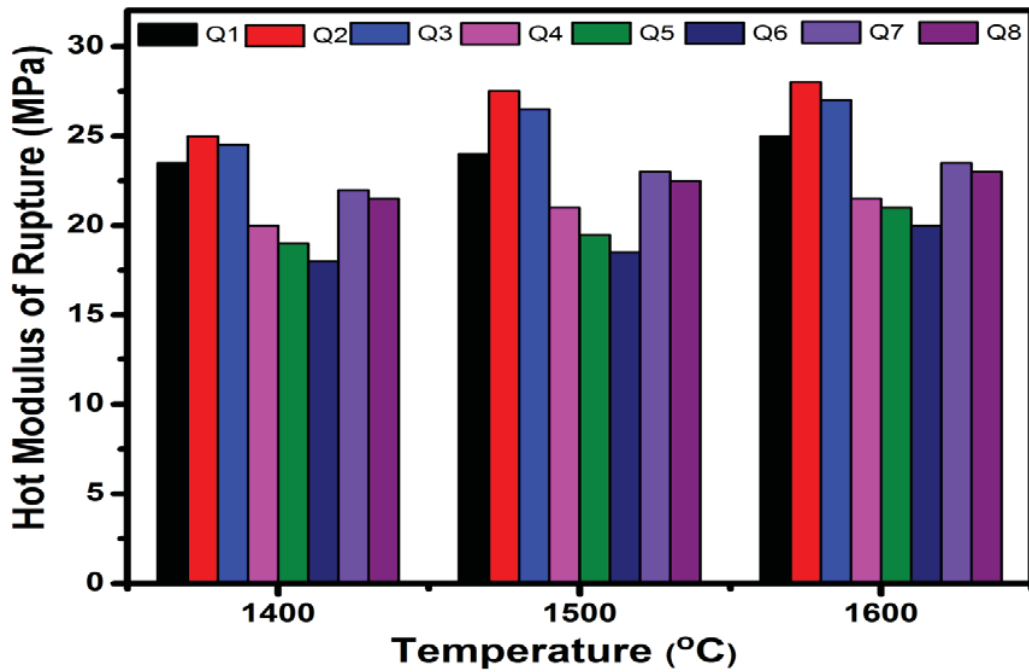

Figure 5.13: Hot modulus of rupture of castables prepared with HAC80.
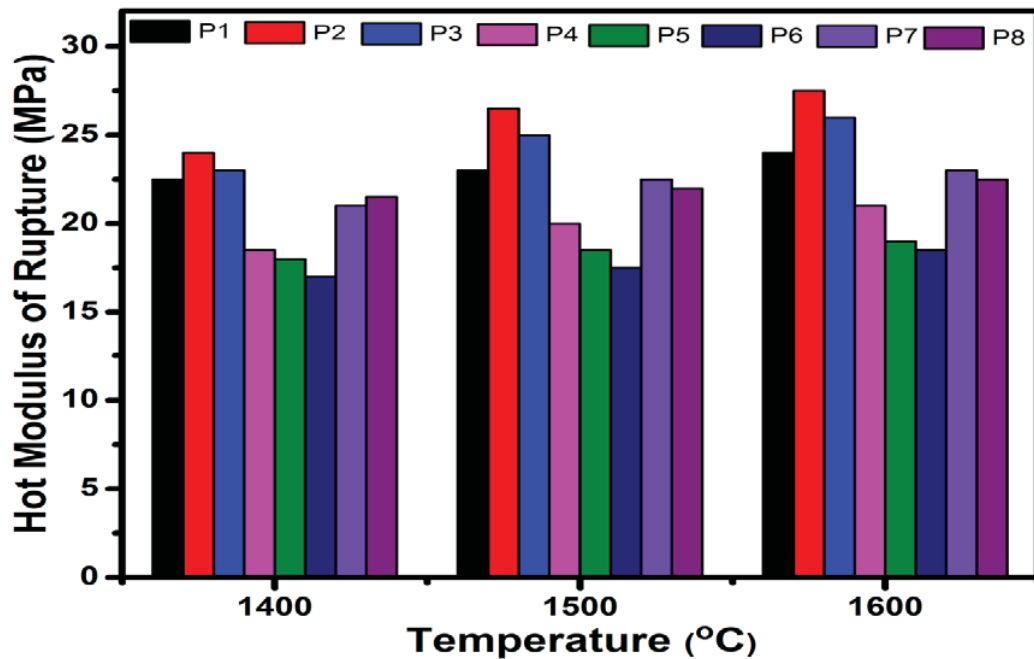
**Figure 5.14: Hot modulus of rupture of castables prepared with HAC70.**

5.3.9 SEM of Q1-Q8 castable

Backscattered images of bauxite based castables are shown in figures 5.15-5.22. The microstructural evolution of castables fired at 1550°C was examined using field emission scanning electron microscopy of representative regions of fractured specimens. Figures 5.15-5.22 depict SEM photomicrographs of Q series castables after firing at 1550 °C for 3 h, where a, b, c and d represent different magnifications. Only Q series castables were chosen for analysis through SEM, as they represented superior thermo-mechanical and physical properties than P series castables. All figures show that all the examined samples have a dense crystalline structure with a high rate of grain growth of spinel as well as direct bonding of the same crystals. The presence of free corundum noticed in all microstructures may hinder the grain growth of round spinel crystals. The high alumina cements bonding phases which were traced in all spinel-based compositions, occur in low amounts, mainly at the grain boundaries of spinel and corundum, so they practically do not reduce the refractoriness of the materials. On the other hand, in samples with MgO and Cr_2O_3

additives, the amount of low melting phases appears to be increasing slightly, but they still are encountered in low amounts. The incorporation of chromium in the spinel lattice helps to increase the rate of strong direct contact between the crystals.

In figures 5.15 and 5.18, the matrix includes CA and some liquid phases. SEM micrographs in figures 5.16 and 5.17 exhibit densely packed microstructure with an abundant face centered cubic spinel grain of comparable sizes, embedded in the trigonal corundum matrix. As we proceed to micrograph figures 5.18 to 5.22, some acicular (needle-shaped) mullite beside corundum grains appeared in the microstructures. The presence of such in-situ formed phase developed as interlocking grains in castables, reinforced the matrix thus confirming the high strength and refractory properties of castables. The microstructures show a very compact and dense microstructure in which the octahedral crystals of magnesium aluminate and magnesium chromite spinels are directly bonded either together or with rounded magnesia crystals. The rod like or elongated crystals, characterizing $[MgO \cdot Al_2O_3 + MgO \cdot Cr_2O_3]$ solid solution, are observed which are bonding spinel-spinel or corundum-spinel crystals together. On the other hand, the impurities that were present in Chinese bauxite could be accounted for a low melting glassy phases, tending to decrease the refractory properties and their microstructure may appear as partially diffused structure in some regions. This property is more evident when we zoom into the microstructures while moving from a to d in each plot. The influence of trace impurities presented during the processing of ceramics is well known and exploited in the control of densification, grain growth and morphology during sintering. The ability to control microstructure is important for achieving desired properties.
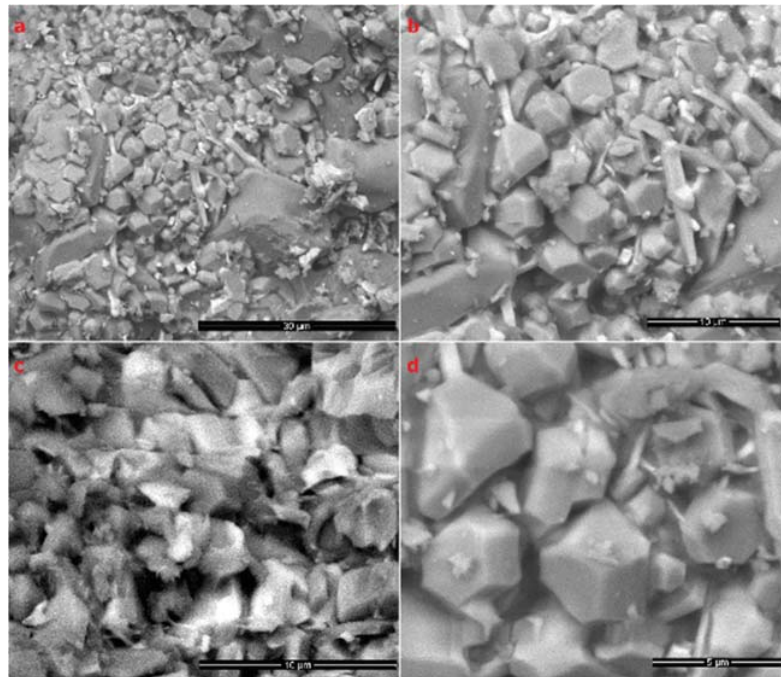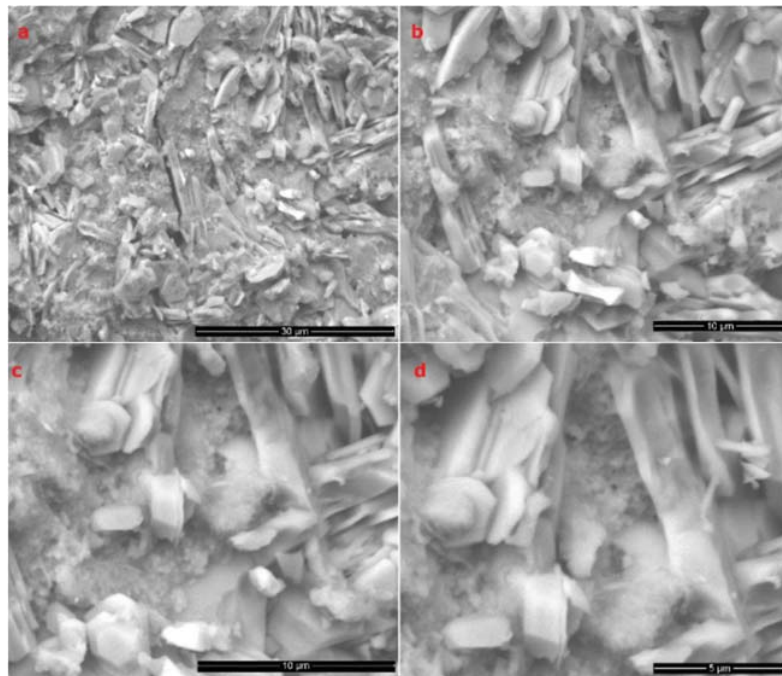
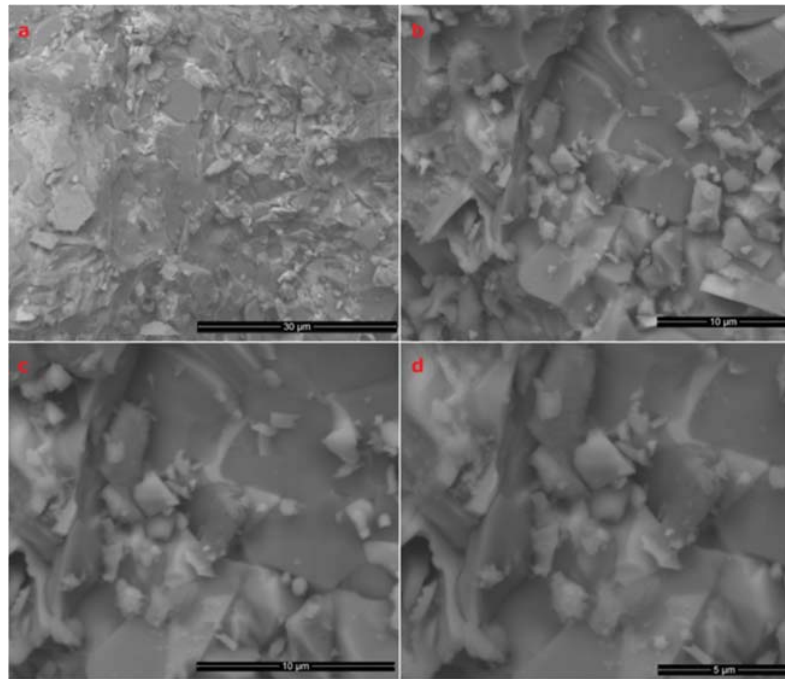**Figure 5.15: SEM of Q1 castable prepared with HAC80.**
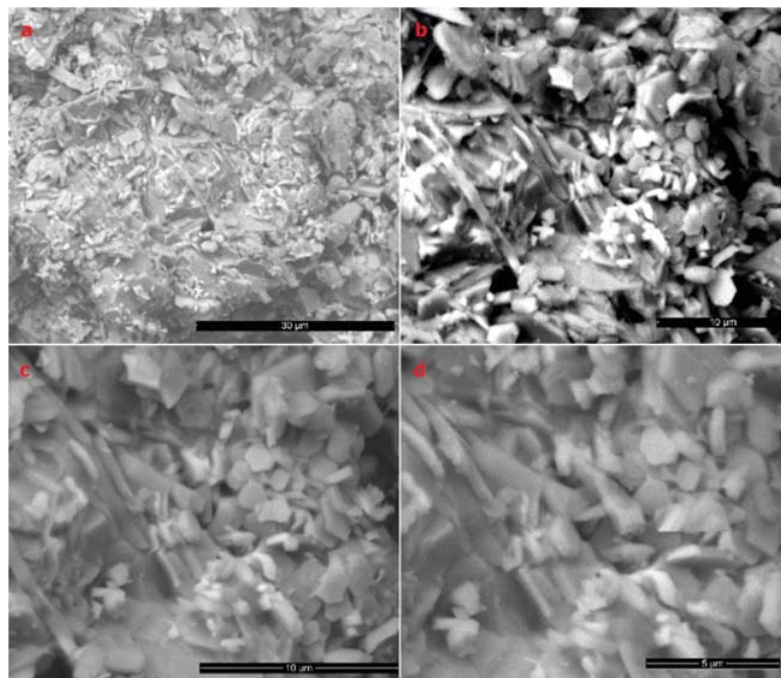
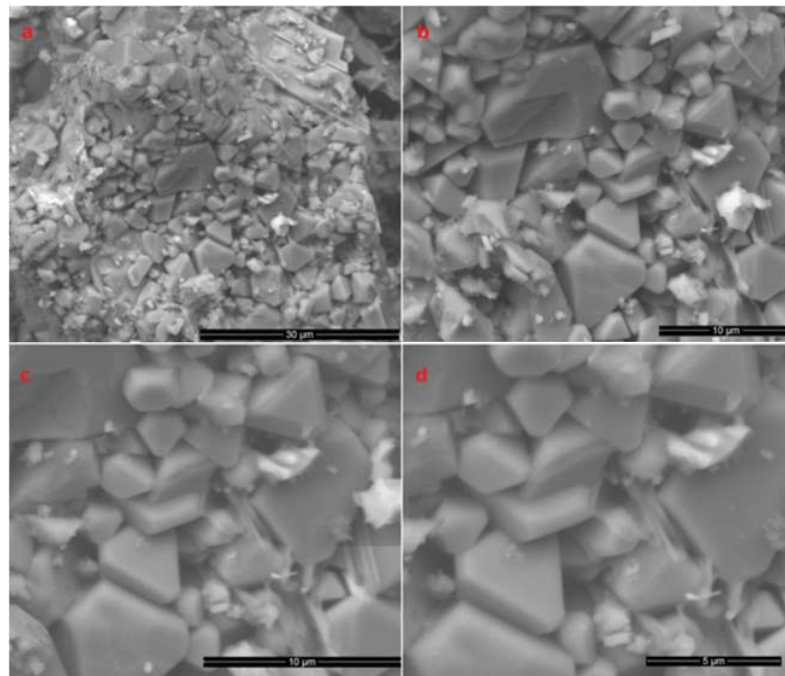**Figure 5.16: SEM of Q2 castable prepared with HAC80.**
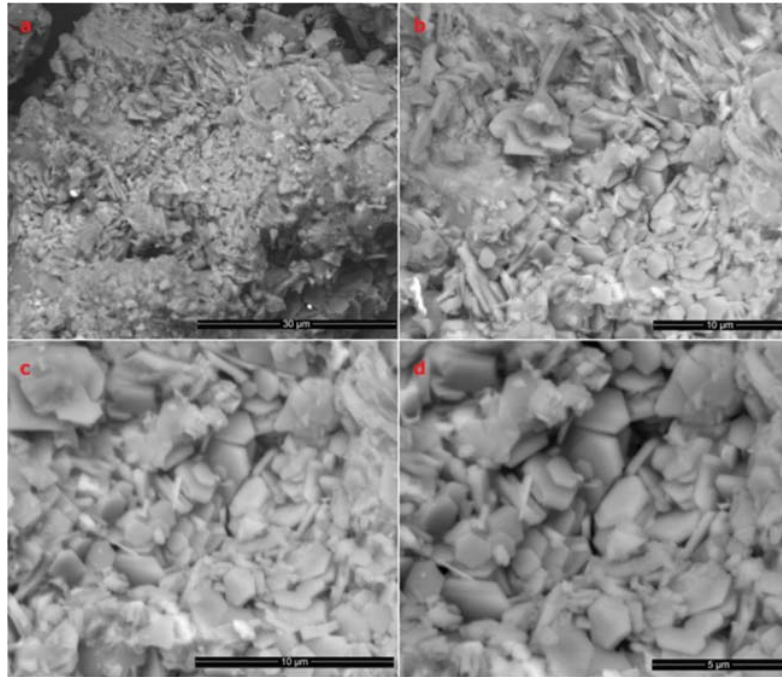
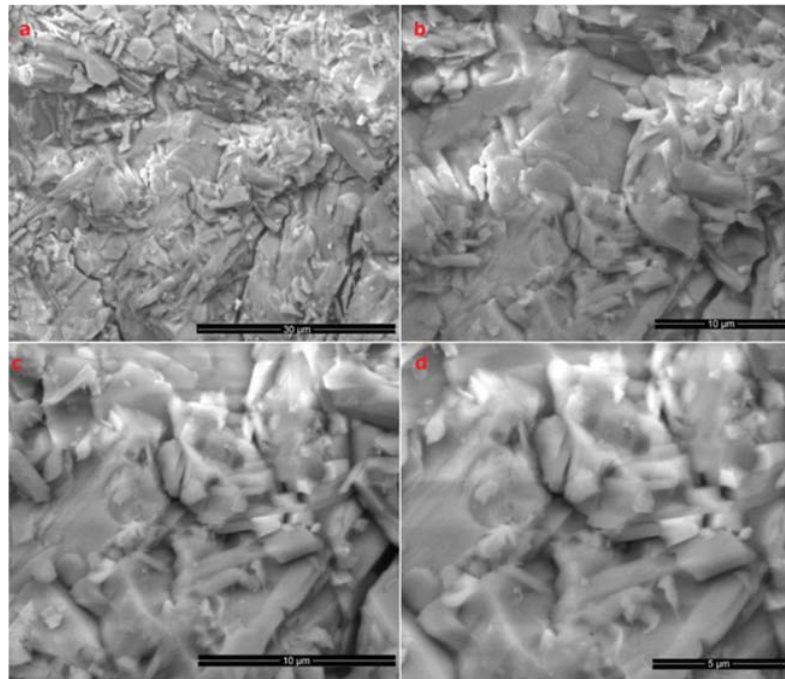**Figure 5.17: SEM of Q3 castable prepared with HAC80.**

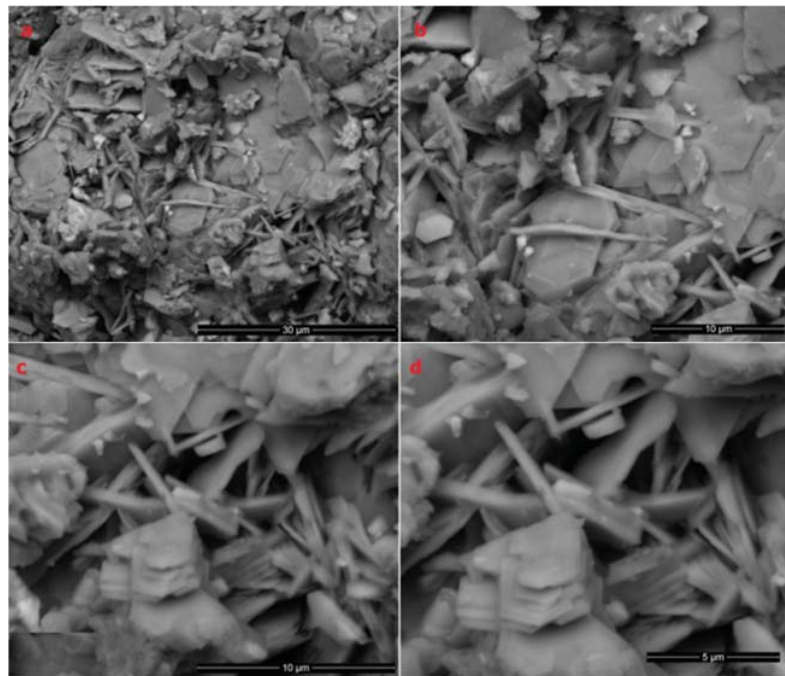**Figure 5.18: SEM of Q4 castable prepared with HAC80.**

Figure 5.19: SEM of Q5 castable prepared with HAC80.

Figure 5.20: SEM of Q6 castable prepared with HAC80.

Figure 5.21: SEM of Q7 castable prepared with HAC80.

Figure 5.22: SEM of Q8 castable prepared with HAC80.

5.4 Conclusions

There have been a lack of conclusive statements on the utilization of auto-combustion processed high alumina cements and their implementations in monoliths and prediction of their high temperature behavior. Our work shows that the combustion synthesis technique is reliable and can be successfully used to produce pure and crystalline calcium aluminates with good compositional control of the powders. Desired cementing phases, having high refractoriness, are identified as CA, CA_2 and $C_{12}A_7$. These were formed at lower temperatures with small crystallite size ranging 18-38 nm. These prepared cements have better physical and cementing properties than their commercial counterparts. One advantage of this process is to produce pure cementing phases and exclude silicates which are the causes behind eutectic formations in such cement bearing castables. These silicate phases decrease the refractoriness and the cement is not suitable for high temperature usage.

The XRD patterns of castables evolved new and pure phases of corundum and spinel. Castable samples prepared by HAC having 80% alumina have better properties than the HAC having 70% alumina. Trigonal corundum and cubic spinel formed at high temperatures facilitate ceramic bonding which were responsible for increase in the CCS and CMOR. Pea sized grains of corundum helped to improve spalling resistance. Dispersion of in-situ formed spinel in fine grained alumina present as a part of castable matrix, promotes its ductile elongation at high temperature and this phenomenon is responsible for high temperature strengths of castables. SEM represents dense microstructure of all the samples and glassy phase appearance is due to the impurities present in bauxite. These excellent properties of castables may enable their uses in various refractory applications, such as fabrication of steel, aluminum, copper, glass, cement, chemicals and ceramics.